Title	Trends in Microstructure Modeling in Weld Metals
Author(s)	David, S. A.; Babu, S. S.; Vitek, J. M.
Citation	Transactions of JWRI. 1996, 25(2), p. 127-143
Version Type	VoR
URL	https://doi.org/10.18910/11851
rights	
Note	

Trends in Microstructure Modeling in Weld Metals*

S. A. David, S. S. Babu, and J. M. Vitek

Metals and Ceramic Division, Oak Ridge National Laboratory
Oak Ridge, TN 37831-6096, USA

ABSTRACT

Various physical processes, such as thermochemical reactions in liquid, solidification, and solid state transformations, control the microstructure development in weld metals. Some fundamental knowledge of the effects of these physical processes on weld microstructure development already exists. However, generalized and integrated models encompassing the current understanding are just evolving. Such models are needed in the design of successful welding procedures for new alloy systems and advanced materials. The principles, methodology, and future directions of modeling weld microstructure development are described in this paper, with examples in low-alloy steel, stainless steel, and Ni-base superalloys. In low alloy steels, the nucleation and growth of oxide inclusions in the melt was modeled as a function of the welding process and composition. This inclusion model has been recently coupled with solidification and numerical heat and mass transfer models. Recent advances in theoretical and physical modeling of the solidification process will be reviewed in this paper with regard to predicting the solidification modes, grain structure development, segregation effects, and nonequilibrium solidification in welds. In nickel-base superalloy welds, the effects of solidification and solid state transformations on microstructure development will be described. In these welds, the final microstructure was found to be dependent on the cooling rates and solidification modes. The weld microstructure was investigated with the help of advanced analytical techniques such as atom-probe field-ion microscopy. The result addresses the importance of advanced analytical techniques in modeling the solid state trans-formation.

1. INTRODUCTION

A fundamental understanding of the welding process is important for a science-based joining design of advanced materials. It is known that coupling of various components of welding, such as welding process selection, process control, process sensing, microstructural evo-lution, and weld properties, is necessary to develop predictive models that can be applied to a wide range of alloy systems and weld geometries. Since these models have to be generalized for new classes of advanced alloys, these models should be based on fundamental principles[1-8]. Although the weld integrity depends on both the heat-affected zone (HAZ) and the fusion zone, the microstructural evolution is more complicated in the weld metal region[1]. The complexity arises due to the gas-plasma-metal interaction, chemical reactions, and phase transformations that occur during the weld thermal cycle. This paper describes current
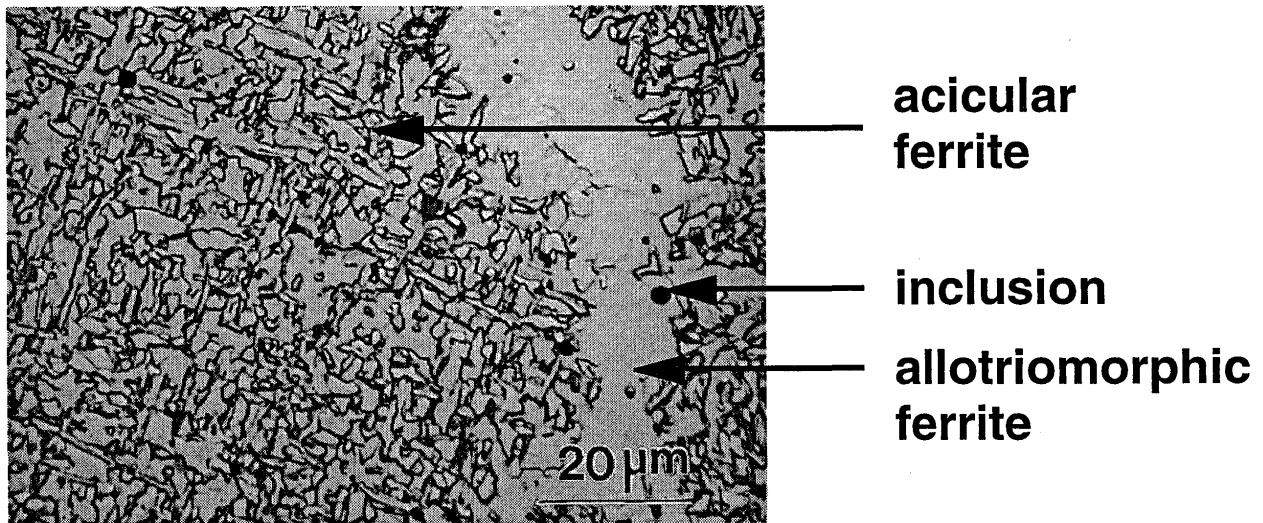

Fig. 1. Typical weld metal microstructure observed in a low–alloy steel weld. The microstructure shows the morphology of acicular ferrite, a desired phase for optimum strength and toughness of welds.

trends in modeling the physical processes that define a typical welding process. This paper also illustrates, with examples, both the complexities of modeling the microstructure development and the importance of advanced analytical techniques as a modeling tool.

2. MODELING FUSION ZONE MICROSTRUCTURE EVOLUTION

A number of physical processes occur during a typical welding operation. They occur in the arc plasma[2-3], weld pool[4-5], and solid state[6-8]. The effect of each of these physical process at high temperatures influences the changes at low temperatures. For example, physical processes such as elemental transport in the weld metal, evaporation of alloying elements from the weld metal, and gas-metal reactions control the final weld metal composition. The weld metal com-position, in turn, controls the microstructure development during solidification and solid state transformations.

An example of the sequential dependency is illustrated with the microstructural evolution in a low-alloy steel weld metal. A typical weld microstructure of a low-alloy steel weld is shown in Fig. 1. The properties of the weld are improved by maximizing the acicular ferrite which exhibits an interlocking and fine micro-structure. Although the acicular ferrite

phase forms from austenite in the 700 to 800 K temperature range, the feasibility of the acicular ferrite formation depends on (a) the presence of inclusions (product of deoxidation in liquid steel in the temperature range 2300 to 1800 K), (b) the austenite grain structure development (tempe-rature range 1400 to 1200 K), (c) the weld metal composition (which is controlled by the gas-metal or slag-metal reaction at temperatures above 1800 K), and the (d) the transformation of austenite to other competing ferrite morpho-logies such as allotriomorphic ferrite and Widmanstätten ferrite. The above sequence is illustrated in Fig. 2. A sequential dependency of microstructure development in the weld metal exists in almost all alloy systems. Therefore, an integrated model, which describes the reactions in liquid state, solidification, and solid state phase transformations, is necessary. General modeling concepts to describe all of these aspects are reviewed below.

2.1 Thermochemical Reactions in Liquid Weld Pool

Thermochemical reactions in the liquid weld pool include evaporation, gas-metal reactions, slag-metal reactions, dissolution of gases, and reaction of dissolved gases with the alloying elements[1]. These reactions are relevant to microstructure development since they control the subsequent solidification and solid
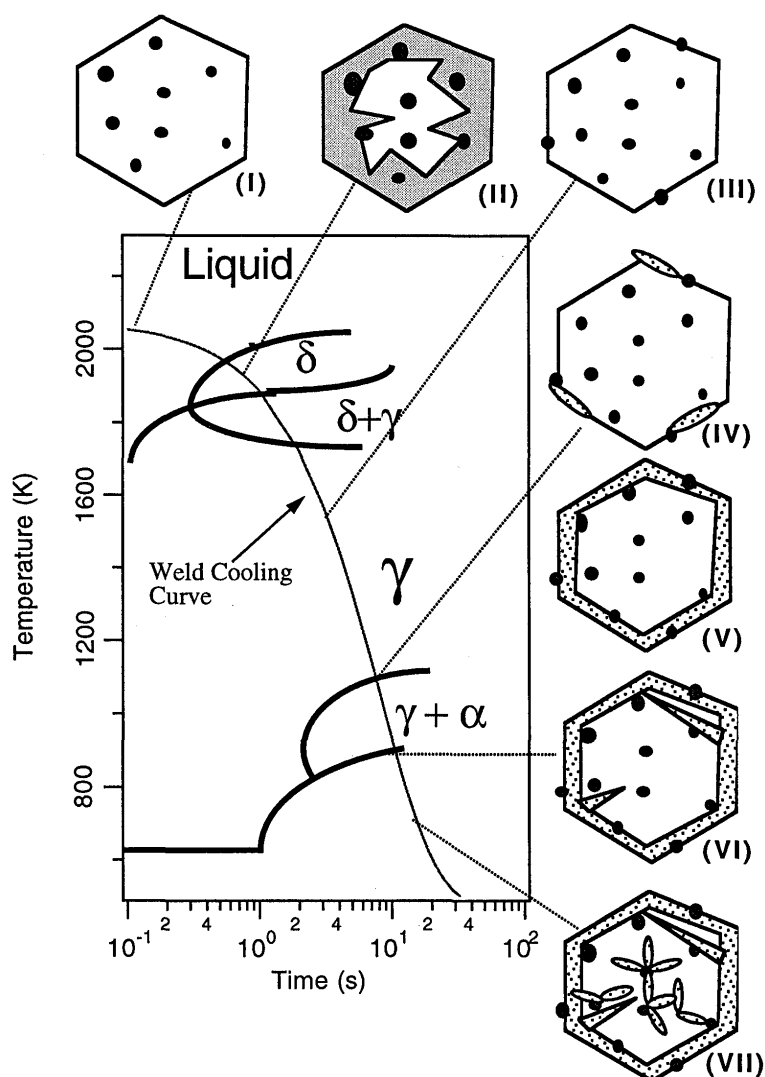
Fig. 2. Schematic diagram of continuous cooling transformation showing the development of weld metal microstructure in low-alloy steels : (I)inclusion formation, (II)solidification of liquid to δ ferrite, (III)fully austenitic structure, (IV)nucleation of allotriomorphic ferrite, (V)growth of allotriomorphic ferrite all along the austenite grain boundaries, (VI)Widmanstätten ferrite formation, and(VII)acicular ferrite formation.

state transformations in welds, as illustrated in the microstructural development in low-alloy steels in the previous section. Detailed modeling activities on the evaporation and dissolution of gases are highlighted in reference 1. These thermochemical reactions are dynamically cou-pled in a typical welding process. For example, the dissolution of oxygen and nitrogen drives the formation of oxide and nitride inclusions, respectively. This nitride or oxide formation, in turn, controls the amount of oxygen and nitrogen that can be dissolved into the liquid steel. Moreover, the plasma conditions around the weld pool, heat transfer, and mass transfer (fluid flow) conditions also affect the formation

of oxides and nitrides. Coupled models that describe the dissolution of gases, thermochemical reaction of the dissolved gases, and alloying elements to form oxides, nitrides, and other compounds are still evolving. The classical equations of the nucleation and the growth of second phase from supersaturated parent phase can be applied to the formation of oxides and nitrides. An example of modeling the inclusion formation will be described later to illustrate the complexity of thermochemical reactions in the liquid steel weld pool.

2.2 Solidification

Weld solidification controls the grain structure, segregation, and defects[5]. Attempts have been made at modeling the weld solidification by extending the current knowledge of the freezing of single crystals, castings, and ingots. In addition, rapid solidification effects in the weld metal are being considered. Modeling of weld or ingot solidification is associated with the nucleation and growth of a solid phase in the liquid. A generalized weld solidification model, besides describing nucleation and growth, must be capable of describing solute distribution, grain structure development, and rapid solidi-fication effects[9-10]. A basic understanding of these concepts is necessary to develop an in-tegrated model capable of describing solid-ification in a wide variety of welding conditions and alloy systems.

During welding, weld pool solidification proceeds from the pre-existing solid substrate without any nucleation barrier. In the case of autogeneous welding, solidification occurs spontaneously by epitaxial growth. In cases where filler metal is used, epitaxial growth may still occur. In addition to heterogeneous nucleation on the solid base material, inoculants have been successfully used to promote nucleation[11]. Other methods to promote nucleation in the weld pool include weld pool stirring and arc oscillations[5] . Although the mechanisms of nucleation in weld metal are well understood, not much attention is given to modeling this phenomenon. Often, weld solidification models assume the epitaxial growth in their models, and for most of the cases, the assumption seems to be appropriate. However, to describe the effect of inoculants, arc oscillations, and weld-pool stirring, heat and mass transfer models[12,13] have to be coupled with either probabilistic models, such as cellular automata (CA)[14-16], or deterministic models using the fundamental equations of nucleation.

The development of microstructural features during the growth of the solid in the weld metal region is controlled by the shape of the solid/liquid interface and its stability. Theories for interface stability under conditions of equilibrium at the interface for normal sol-

idi-fication, or under extreme nonequili-brium conditions prevalent during rapid solidification, have been developed[17-18]. These theories can be extended to weld pool solidification. The parameters that determine the solidification micro- structure in castings are growth rate (R_S), temperature gradient (G), undercooling (ΔT_U), and alloy composition. It is well known that the temperature gradient and growth rate are important in the combined forms GR_S (cooling rate) and G/R_S since they influence the scale of the solidification substructure and the solidification morphology, respectively. In welding, where the molten pool moves through the material, both G and GR_S vary considerably across the weld pool region. Figure 3 shows schematically the influence of G and R_S on the microstructural variations within the weld metal. The figure shows the regions of planar to cellular transition (PCT) and cellular to equiaxed transition (CET).

The method of using GR_S and G/R_S relations to depict the solidification morphology has proved to be simple and elegant. However, modeling of solidification morphology in a typical weld must consider other factors such as the fluid flow, the density of grains at the fusion line taking part in the epitaxial growth, the effect of base plate texture on the growth patterns in the weld metal region[16, 19], and the amount of total undercooling (ΔT). Although the CA models[14, 16] can be used for modeling the spatial morphology and transitions from cellular to equiaxed solidification in casting processes, much work needs to be done in improving the extension of this method to welds[16]. Future solidification morphology models, such as CA techniques, should consider solute diffusion, and the models should be coupled with the numerical models that consider the diffusion of partitioned alloying elements between solid and liquid phases[20,21].

Solute distribution during weld pool solidification is an important phenomenon resulting in segregation that can significantly affect weldability, microstructure, and pro perties. Various studies on extending different solidification models to describe solute distribution have been summarized[5]. In describing the solute distribution under dendritic growth conditions, consideration should be given to
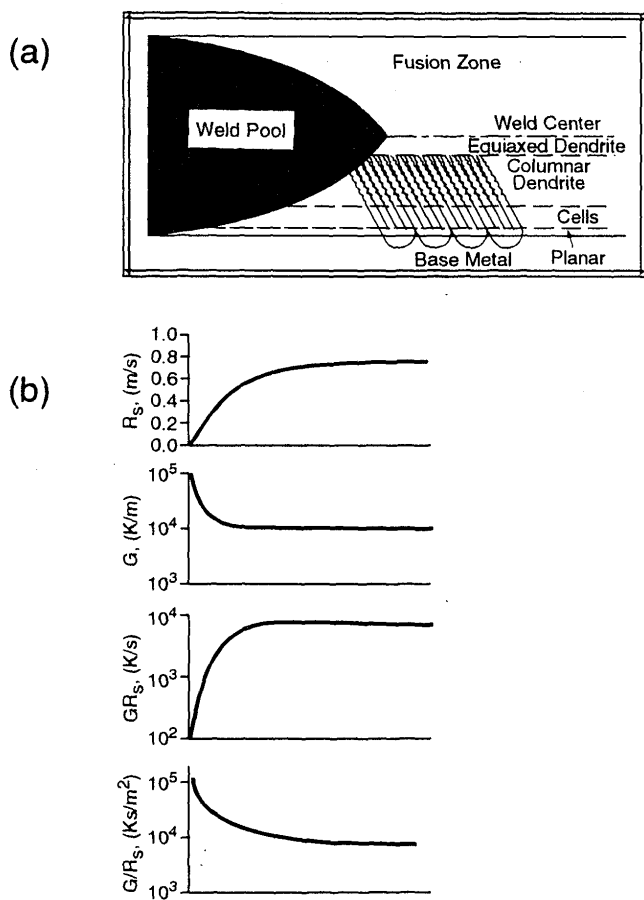
(a)

(b)

Fig. 3. (a) Schematic illustration of weld microstructure across the fusion zone and (b) corresponding schematic variation of G, Rs, GRs, and G/Rs values as a function of position.

drite tip undercooling has been found to be significant (3 to 8.5°C). Considering the solute redistribution in the interdendritic regions, it may be sufficient to extend the solidification model for micro-segregation in castings to welds. In such cases, the weld solidification models can assume little or no diffusion in the solid while complete mixing of solutes in the liquid by convection can be assumed. This can be achieved by the Scheil equation[22] or modified Scheil equations that consider the diffusion[20,21] in the solid during welding.

During welding, the growth of solid often occurs by epitaxial growth from the partially melted grains in the base metal. Therefore, the weld metal grain structure is predominantly determined by the base metal grain structure and the welding conditions. In addition, crystallographic growth competition will influence the grain structure development. It is well known that grain growth into the liquid region is favored along easy growth crystallographic directions, for example <100> in cubic metals. Conditions for growth are optimum when one of the easy growth directions coincides with the heat flow direction. Since the solid/liquid interface is essentially perpendicular to the heat flow di-rection, the pool shape influences the optimum growth direction. Using a recently developed geometrical analysis and expressing the solidi-fication front normal and the crystallographic growth directions in terms of a fixed set of reference axes, the dendrite growth selection process in Fe-Ni-Cr single-crystal welds was evaluated[23-26]. This analysis can also be extended for the grain growth selection process. These types of geometrical models can also be used to describe the three-dimensional (3-D) reconstru-ction of the weld pool shape.

With the increased use of high-energy beam processes, such as electron and laser beams, for welding, observations of nonequilibrium microstructures under rapid cooling conditions are becoming common. Such observations are well documented for austenitic stainless steel welds[27-31]. Modeling of the transition in weld grain structure due to rapid solidification is just evolving. Under rapid cooling conditions, a significant departure from local equilibrium at the solid/liquid interface may occur. As a result, nonequilibrium structure and,

redistribution at the dendrite tip and in the interdendritic regions. The solute distribution at the dendrite tip is determined, to a large extent, by the dendrite tip undercooling, which is made up of four components: thermal undercooling, kinetic undercooling, constitutional undercooling, and undercooling due to tip curvature[5]. In welding, the first two contributions can be ignored. However, since the microstructures are much finer in scale in welds than in castings, the contribution to the total tip undercooling due to the curvature effect is very significant[5,20]. The effect of increased under-cooling at the dendrite tip would be to solidify at a composition closer to the overall composition and thus reduce the extent of microsegregation. Dendrite tip under-der-coolings in welds have been estimated by measuring dendrite core compositions in two different alloy systems, Al-Cu and Fe-Nb, after gas tungsten arc welding[20]. The estimated den-
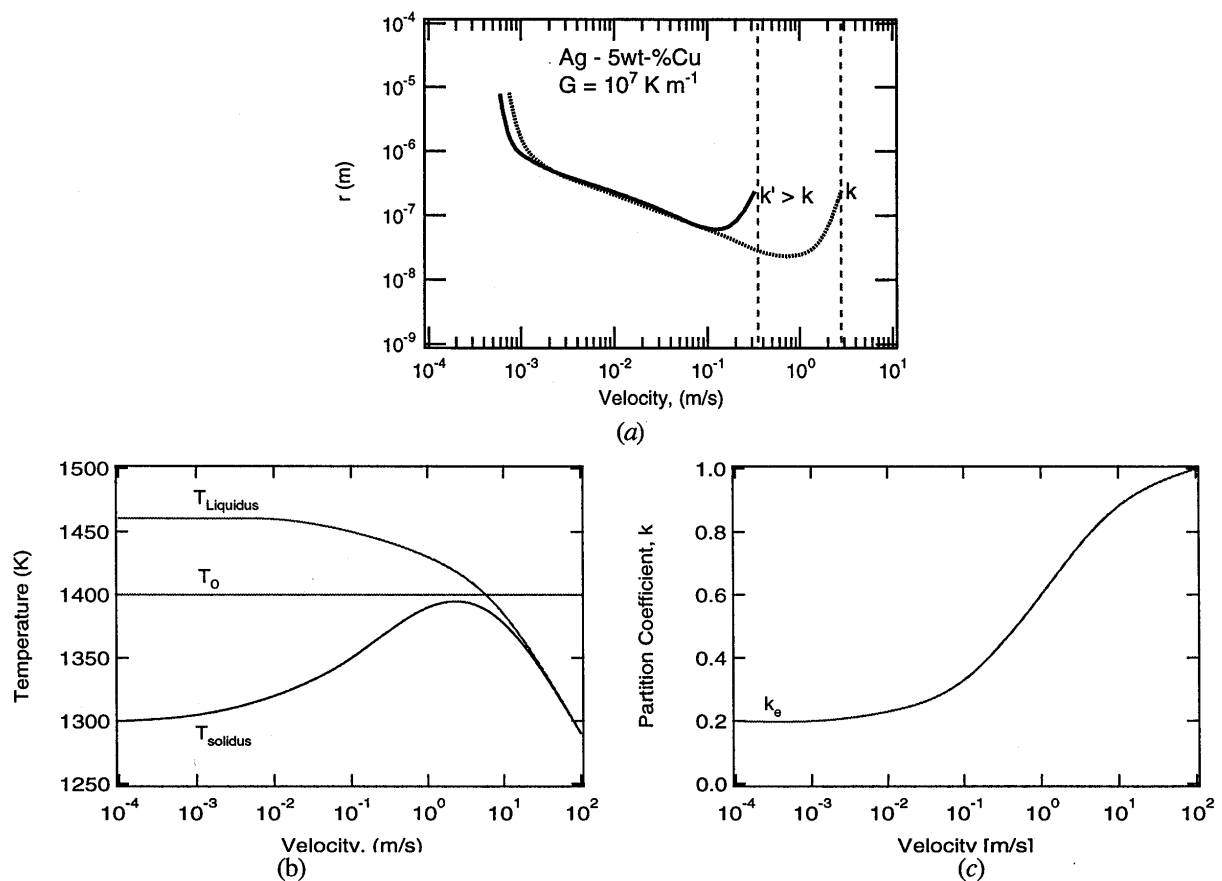
Fig. 4. (a) Effect of velocity–dependent partition coefficient on dependence of dendrite tip radius (r) on growth velocity [5], (b) variation of nonequilibrium solidus and liquidus temperatures, and (c) partition coefficient as a function of growth velocity in a Fe–base alloy [32].

in some cases, partitionless solidification can be observed. The magnitude of these departures is not fully understood and characterized. Another con-sequence of rapid solidification conditions is that plane front solidification may become stable at extremely rapid growth rates as illustrated in Fig. 4 (a)[5]. An additional effect of rapid solid-ification is the change in the liquidus and solidus temperatures as illustrated in Fig. 4(b)-(c)[32]. In summary, the integrated weld solidification models must describe the transition from clas-sical to rapid solidification in a generalized form.

2.3 Solid State Transformations

In some alloys, the solid state transformations that occur in the weld metal region control the final microstructure and properties, as seen in the case of low-alloy steel welds. Therefore, modeling solid state transformations in welds is important in developing generalized,

integrated models for weld metal microstructure development. In this section, various models that deal with the solid state transformation and that describe the microstructural development are briefly summarized, and the need for further improvement in the models is highlighted.

Significant work has been carried out on modeling the solid state phase transformation in the HAZs[8]. Recently, much attention has been given to modeling the microstructure in weld metal regions[7]. In addition to phase transformations in solid state during weld thermal cycles, an integrated model for microstructure development should consider other solid state phase changes such as grain growth, coarsening, and solute redistribution. Most of the recent work has concentrated on describing the solid state phase transformations with fundamental theories of phase transformations[7,8,33] Various solid state transformations that occur in welds during welding and in service can be grouped

into four categories as follows: (1) phase changes in-volving diffusional processes such as pre-cipitation or dissolution of the second phase in the matrix; (2) solid state processes involving grain growth[34-36], precipitate coarsening, and single-phase solute redistribution[37]; (3) phase changes involving displacive transformations such as martensitic transformations ; and (4) phase changes such as spinodal decomposition[38]. Moreover, it is important to note that some of the above phase changes may occur concurrently and interact with each other. Therefore, a prior knowledge of various phase transformations that occur in an alloy system is necessary before developing a model for weld metal micro- structure development.

Some of the solid state phase changes that occur in welds can be described by diffusional processes. Some examples of diffusional proc-esses are austenite to allotriomorphic ferrite transformation in steel welds, dissolution of carbonitride precipitates in steel welds, and de-composition of primary ferrite into duplex austenite-ferrite microstructure in austenitic stainless steels. In principle, modeling of diffusion controlled phase transformation involves describing the kinetics of phase change with nucleation[39] and the growth/dissolution of second phase in a matrix[40]. The growth/ dissolution of second phase in the matrix can be modeled with the assumption of local equilibrium at the second phase/matrix interface. Often, a thermodynamic description of equilibrium at the growth interface is obtained from published thermodynamic data. In some cases, the models describing diffusional phase changes must be coupled with models of other solid state changes, e.g., the grain growth can be controlled by the concurrent precipitation or dissolution of precipitates[36].

Other solid state changes that occur in welds which are driven by minimization of interfacial energy' are grain growth and coarsening. Grain growth in welds is either modeled by analytical equations[36] or by Monte Carlo (MC) simulations[34,35,41,42]. A typical example of isothermal grain growth simulation is shown in Fig.5(a)[41,42]. The same methodology can be applied to 3-D grain growth also [see Fig. 5(b)]. The reader is referred to published literature[41,42] for more details of the simulation. A specific advantage of MC simulations is the capability to describe the 3-D morphology of grains during the grain growth process, as observed in the images shown in Fig. 5. Despite the success of MC simulation in describing the grain morphology, until recently, there were no proven methods for a one-to-one correlation between simulated measures of grain size and time with experimental measures. Recently, Radhakrishnan[42] addressed the above issue and suggested a general method of deriving a one-to-one correlation between experiments and simulation. In addition, the MC simulations can illustrate the effects of steep thermal gradients across a grain. In addition to this probabilistic MC simulation approach, recently, Grong[43] has suggested an internal state variable approach for modeling solid state transformations including grain growth in welds.

Displacive transformations occur in many steel welds, e.g., transformation of austenite to Widmanstätten ferrite, acicular ferrite, bainite, and martensite[44]. An approximate kinetic model for bainite formation has been coupled with the cooling rates in welds to model the formation of local-brittle zones in welds[45]. It is also note-worthy that the displacive transformation kinetics and transformation morphologies are quite sensitive to the presence of external or internal stresses on welds. Upon application of elastic stresses during transformation from austenite to acicular ferrite, a change in the morphology of acicular ferrite plates and trans-formation-induced plasticity was obser-ved[46]. This observation has to be studied further and must be modeled in order to understand the interaction between microstructure and residual stress development in welds.

Spinodal decomposition has been reported in duplex austenite-ferrite microstructures of thermally aged stainless steel welds[38]. In this case, the spinodal decomposition occurs in the ferrite phase upon aging at 748 K, with the ferrite decomposing into Cr- and Fe-rich regions. The initial composition of ferrite and the aging temperature control the kinetics and feasibility of the spinodal decomposition. In this case, it is desirable to couple thermodynamic software[46] with either numerical[21,47] or analytical models of weld metal microstructure
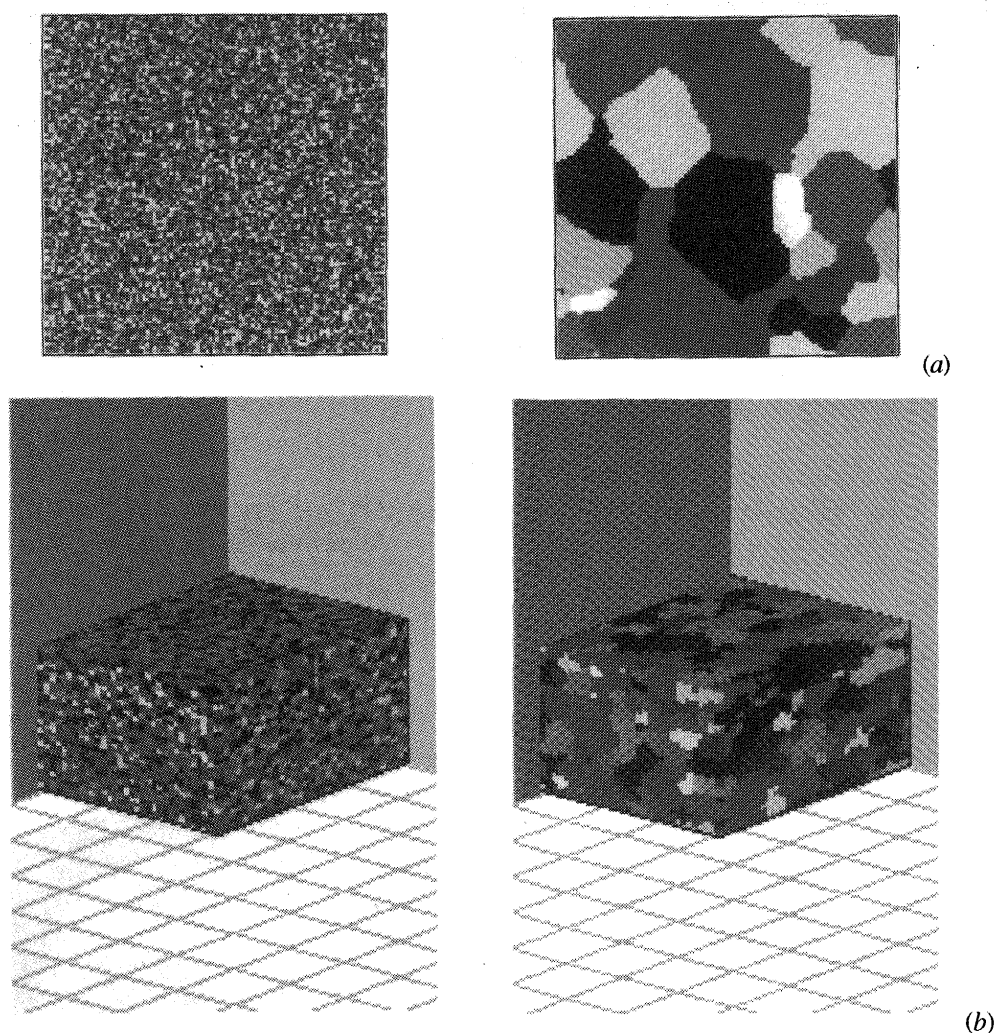
(a)

(b)

Fig. 5. Results of Monte Carlo grain growth simulations as a function of Monte Carlo Simulation Steps (MCS) : (a) Two-dimensional simulation (the graph shows the simulated grain structure at 0 and 100 MCS done on 50 by 50 square grid with 64 initial random orientations) and (b) Three-dimensional simulation of the grain structure at 0 and 75 MCS done on $32 \times 32 \times 32$ cubic grid with 64 initial random orientations. The details of the method are in the published literature [41, 42].

development.

In summary, the first step for an integrated and generalized model for describing solid state transformation is the identification of key transformations and their mechanisms in a given alloy system that may control the microstructure development. The next step in the model involves the coupling of models for diffusional decom-position, grain growth, coarsening, displacive transformation, and spinodal decomposition based on the feasibility of each reaction. Finally, these coupled models have to be interfaced with models for weld thermal history.

3. EXAMPLES

3.1 Modeling Inclusion Formation in Steel Welds

In general, inclusions form in low-alloy steel welds due to the reaction between the dissolved gases and other elements in the liquid steel. The oxide inclusion formation is controlled by the concentrations of dissolved oxygen and deoxidizing elements, such as aluminum, titanium, silicon, and manganese. The dis-solution of oxygen into the liquid steel is affected by the arc-atmosphere conditions around the molten steel. For example, it is

known that the dissociation of diatomic gases into monatomic species affects the dissolution of gases into liquid steel[48,49]. The important inclusion characteristics are inclusion composition, size, and number density. Other important aspects related to inclusion formation are the oxidation sequence and the concentration of residual deoxidizing elements[50-52]. The residual deox-idizing elements in solid solution, such as Al, Ti, Si and Mn, that remain after the oxidation reaction influence the transformation of aus-tenite to ferrite at lower temperatures. Previous attempts[7,50,51] to predict inclusion composition assumed a fixed oxidation sequence of Al_2O_3, Ti_2O_3, SiO_2, and MnO. This assumption was based on the ranking of the oxides Al_2O_3, Ti_2O_3 (or to other types of Ti_xO_y oxides), SiO_2, and MnO according to their standard free energy of formation. However, the oxidation sequence may change as a function of the concentrations of reacting elements. More-over, previous work did not model other inclusion parameters such as inclusion number density, size, and residual amounts of de-oxidizing elements. In addition, the complexity of the solidification-induced sulfide and oxide formation was ignored. In this work, inclusion formation is described in two stages (1) the oxide inclusion formation in the liquid steel in the temperature range of 2300 to 1800K and (2) during solidification. In the first stage, the inclusions are mainly oxides, and in the later stage, the main consideration is sulfide formation. The multicomponent partitioning and sulfide formation are treated with ThermoCalc™ software[46] using a published computing routine described later[21]. The steps involved in the inclusion calculations are shown in a flow chart given in **Fig.6**.

3.1.1 Overall Oxidation Kinetics in Liquid Steel:

Inclusion formation in the liquid steel will be controlled by the rate at which the weld cools and oxidation kinetics. The steps involved in the present calculation are as follows: (1) deter-mining driving force for oxide formation, (2) calculate homogeneous nucleation rates, (3) calculate growth rates, and (4) calculate overall oxidation kinetics as a function of temperature and composition. The methodologies for each of the above calculations are published else-

where[52]. The isothermal oxidation kinetics calculations are then applied to the continuous cooling conditions.

The overall isothermal oxidation kinetics at a particular temperature Ti involving a deoxidizing element (M) and oxygen (O) dis-solved in liquid steel to produce an oxide inclusion of M_xO_y is given by the following equation[52]:

$$\zeta = 1 - \exp\left\{-\left((8\pi/15)I_V\left(\alpha_3^*\right)^3 t^{\frac{5}{2}}/\Omega\right)\right\} \qquad (1)$$

where ζ is the extent of reaction (varying from o at start to 1 at finish), I_V is the homogeneous nucleation rate of oxide M_xO_y per unit volume per second, α_3^* is the parabolic thickening rate of oxides in liquid steel, t is the time of reaction at temperature T_1, and Ω is the equilibrium volume fraction of M_xO_y at T_1, given by:

$$\Omega = \left(c_{\underline{M}}^l - c_{\underline{M}}^{il}\right)/\left(c_{\underline{M}}^i - c_{\underline{M}}^{il}\right) \qquad (2)$$

where $c_{\underline{M}}^l$ is the average (overall) concentration of the deoxidizing element, $c_{\underline{M}}^{il}$ is the concentration of deoxidizing element in the liquid in equilibrium with the inclusion, and c_M^i is the concentration of deoxidizing element in the inclusion in equilibrium with the liquid. The equilibrium concentration of deoxidizing element, c_M^{il}, is obtained from the tie line in the deoxidation phase diagram (the concentrations are in mole fraction). The expressions for calculating other terms α_3^*; and I_V are given elsewhere[52]. Equation (1) enables one to predict the isothermal oxidation kinetics for various oxides as a function of nominal composition and temperature. Isothermal oxidation kinetics calculations were applied to continuous cooling conditions. The integrated number density of the first-forming oxide was taken as the final number density of inclusions in the steel weld (this assumption is based on the observation of heterogeneous and layered inclusion struc-tures)[50]. The calculation of final inclusion number density is given by:
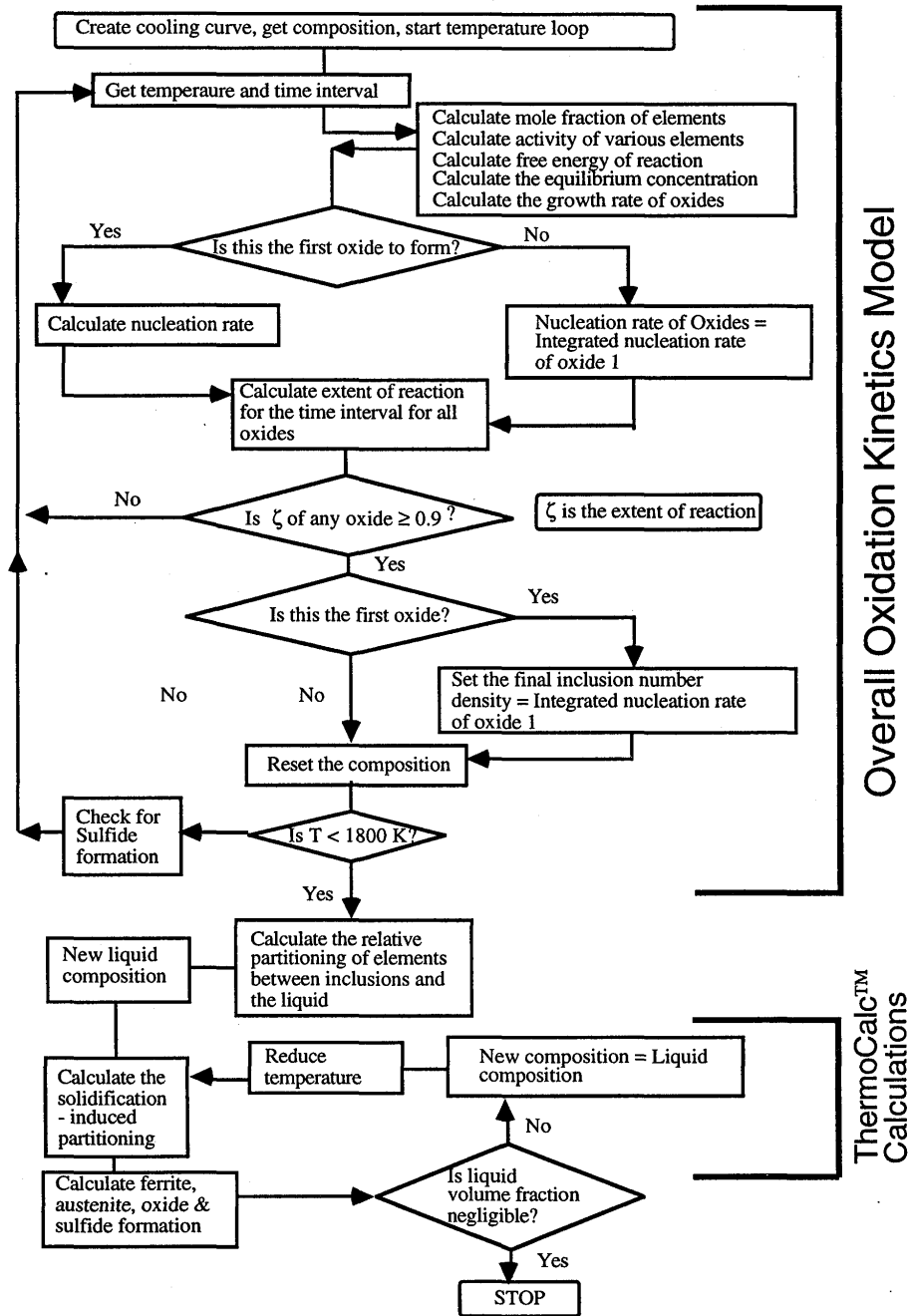
Fig. 6. Flow chart illustrating the application of isothermal oxidation kinetics calculations to continuous cooling conditions. The calculation starts with a nominal weld composition at 2300K. The cooling curves are then divided into small isothermal steps. The kinetic calculations are performed at each temperature and time interval, and additivity of oxide volume fraction is assumed. The flow chart also illustrates the steps to calculate the effect of solidification on inclusion formation.

$$Number\ Density = \sum_{i=T_{start}}^{i=T_{end}} I_V^{oxide1} \times \Delta t_i, \qquad (3)$$

Where $I_V^{oxide\ 1}$ is the nucleation rate of the first-forming oxide as a function of temperature; and Δt_i is the time spent at each temperature from T_{start} the temperature at which the first oxide starts to form, to T_{end}, the temperature at which the extent of reaction, ζ, of the first oxide reaches 0.9. The accumulated volume fraction of oxide inclusions at the liquidus temperature was taken as the final volume fraction of oxides, and the residual liquid com-
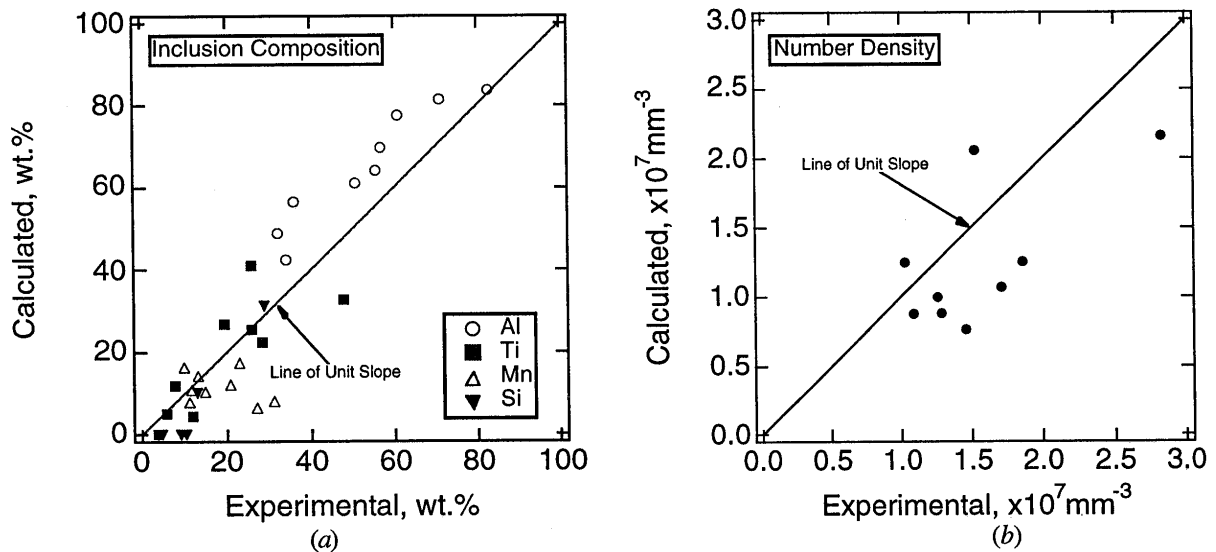
Fig. 7. Comparison of experimental inclusion characteristics measured by Kluken and Grong [50] and the calculated inclusion characteristics by the present inclusion model : (a) inclusion composition and (b) inclusion number density.

position at 1800 K was related to the amount of deoxidizing elements in solid solution. With the knowledge of the final inclusion volume fraction (V_f) and final number density, the average inclusion radius was calculated.

3.1.2 Overall Oxidation Kinetics Model Validation:

The overall oxidation kinetics model developed in this work was validated with experimental results. The cooling rate data necessary for the calculation of inclusion characteristics were obtained by using the equation given by Ion et al[36]. However, it is important to note that these cooling rate calculations are approximate, and, ideally, one should use the weld metal cooling rate calculations which consider the heat flow and mass transfer in the weld pool region[53]. To improve the predictions of the number density, enhanced thermal conductivity (2.25 times the original thermal conductivity value given in the reference 36) values were used. The calculations were validated with the experimental data of Kluken and Grong[50]. A comparison of experimental results of inclusion composition and final number density published by Kluken and Grong[50] with the calculations of the present inclusion model is shown in Fig. 7. The comparison shows that the present inclusion model predicts a trend similar to that of the experimental data. However, the predictions are

not exact. The comparison of experimental measurement and theoretical estimation of aluminum in solid solution showed only a fair correlation[54]. However, excellent agreement is observed with the predicted titanium levels in solid solution. The calculations showed that most of the oxygen is tied up as oxides as the liquid cools to 1800 K. Moreover, the model showed that no sulfides formed above 1800 K due to low supersaturation. However, it is known that in almost all steel welds some amount of sulfide reaction forms during the final stages of solidification, due to solute enrichment. Therefore, the next part of the inclusion calculations considers the feasibility of sulfide formation, considering the multicomponent partitioning between liquid and solid, during solidification.

3.1.3 Effect of Partitioning During: Solidification;

During low-alloy steel solidification, alloying elements partition between liquid and solid. It is also known that due to the partitioning, the liquid gets enriched progressively with elements which have low solubility in the solids as the solidification continues,. This enrichment results in a higher supersaturation sufficient to initiate some reaction which would not occur with the nominal composition of the weld. Various models have been developed

to describe this solute partitioning as mentioned in the earlier section. In the present work, a published model to calculate inclusion formation during stainless steel solidification was applied to the low-alloy steel welds. In this model, complete mixing in liquid and some amount of diffusion in solid are assumed, and the volume fraction of liquid and solid is given by equilibrium calculations. The diffusion in solid was considered using a modified Clyne and Kurz equation[21]. However, the partitioning coefficient of each element is calculated in an iterative manner at each temperature interval using ThermoCalc[TM] software. This allows for the consideration of the partitioning coefficient in a multicomponent system, instead of simply using the partitioning coefficients from binary alloy systems. The steps are explained in Fig. 6. The governing equations are given below:

$$\Delta C_{liquid,C-K} = \frac{(1-f_s)}{\{(1-f_s)+2\Omega f_s k\}}\Delta C_{liquid,\Delta Temp},$$

(4)

where $\Delta C_{liquid,C-K}$ is the effective change in liquid composition after considering the solute diffusion in solid with a change in temperature, $\Delta C_{liquid,\Delta Temp}$ is the calculated equilibrium change in liquid composition without considering the solute diffusion in the liquid, f_s is the volume fraction of solid, k is the partitioning coefficient of a corresponding element at a particular temperature, and Ω is given by:

$$\Omega = \alpha \left[1-\exp\left(-\frac{1}{\alpha}\right)-0.5\exp\left(-\frac{1}{2\alpha}\right)\right]$$ (5)

and

$$\alpha = \frac{4Dt_S}{L^2},$$ (6)

where D is the diffusivity of a particular element, t_S is the time spent at a particular temperature and L is the interdendritic spacing.

The validity of the above model to describe the sulfide formation was tested by applying the calculations to some of the weld compositions given in reference 50. The final composition obtained after the overall oxidation kinetics model was applied to the solidification calculation as a function of tem-

perature. A cooling rate of $10\,^\circ C\,s^{-1}$ and an interdendritic spacing of $1\,\mu m$ were assumed for all welds. These values are assumed only to demonstrate the suitability of the above method. In addition to the sulfide formation, the calculations showed a small amount of oxide formation. The amount of oxides was related to the oxygen concentration of the liquid after the completion of earlier oxidation above 1800 K. The changes in the volume fraction of the solid, liquid, oxide inclusions, and sulfide are stored as a function of temperature while considering the cooling of the weld at $10\,^\circ C\,s^{-1}$ The calculated changes in the volume fraction of the solid, liquid, and MnS for a given composition are shown in Fig. 8(a). The variations of MnS fraction for various nominal concentrations of sulfur are shown in Fig. 8(b). The calculations showed no systematic variation of MnS formation as a function of nominal sulfur concentration. This was attributed to the co-precipitation of other oxides and complex sequences of oxide and sulfide formation. Although the present model is capable of describing the solidification-induced sulfide formation, more improvements are necessary to consider the diffusion of elements in liquid. The assumption of complete mixing in liquid may not be valid at other rapid weld cooling conditions. Further work is under way to describe diffusion in both the solid and liquid using coupled thermodynamic and kinetic models.

3. 1.4   Future Directions;

Although the inclusion model is capable of describing the inclusion formation in steel welds, there are limitations in the present model. To improve the cooling rate expressions in the liquid steel weld metal region, ongoing work focuses on coupling heat transfer and the fluid flow calculation method developed by Mundra et al[53]. The predicted values seem to be comparable to those of experimental data. Moreover, recent experimental work has shown that fluid flow in liquid steel plays a vital role in determining the ultimate inclusion number density[53]. Therefore, future improvements may be achieved by using a particle tracking approach to track the inclusion coarsening in steel weld metal.

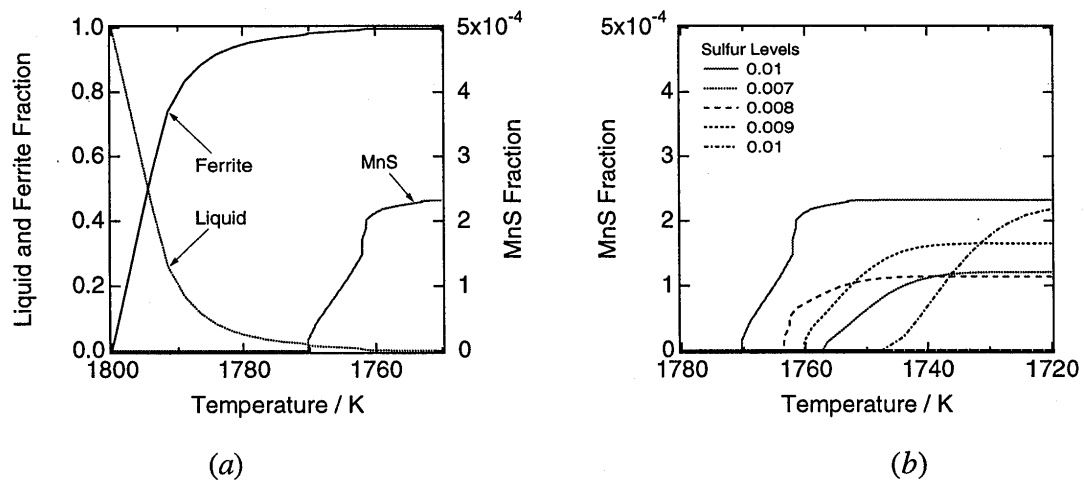(a)   (b)

Fig. 8. (a) Change in the volume fraction of liquid, ferrite, and MnS as a function of weld cooling. The initial rapid increase and the saturation of the volume fraction of MnS as a function of temperature indicates the initial increase in supersaturation of sulfur in liquid and the depletion of sulfur due to the formation of MnS, respectively. (b) The change in volume fraction of MnS as a function of solidification temperature for various nominal concentrations of sulfur in welds. The absence of monotonic relation is attributed to co-precipitation of other oxides in addition to sulfides.
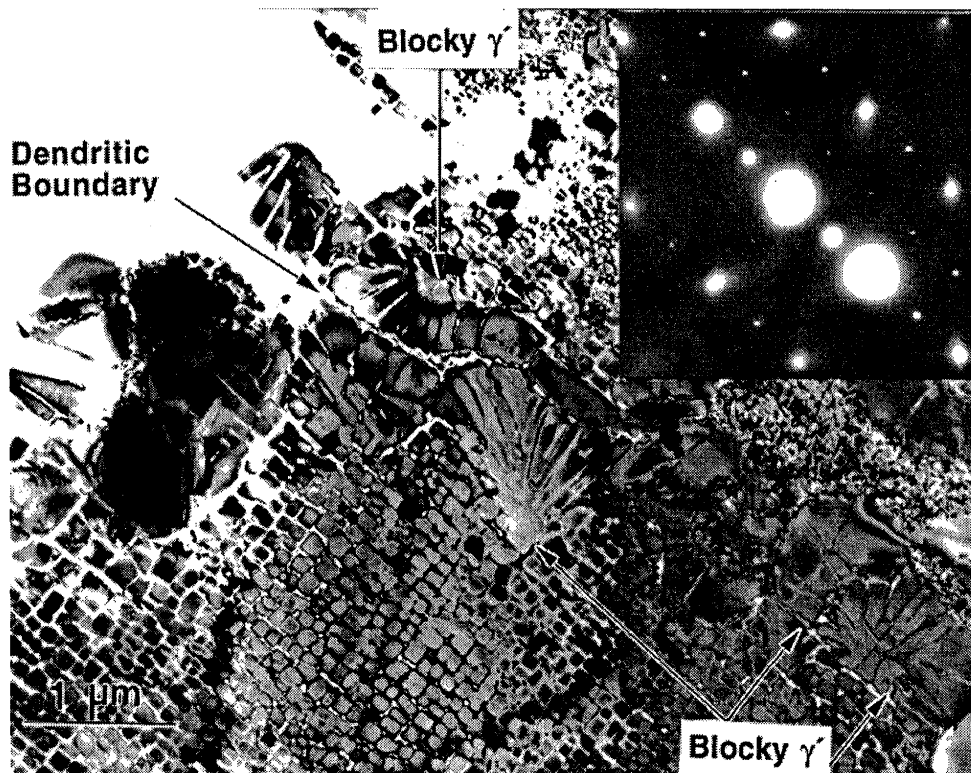

Fig. 9. Transmission electron micrograph of the PWA−1480 weld metal region in the as−welded condition showing dendritic boundary and eutectic γ' precipitate (marked by an arrow) along the dendritic boundary. The electron diffraction pattern (inset), taken near to the [001] γ zone, shows the superlattice reflections from γ' precipitates.
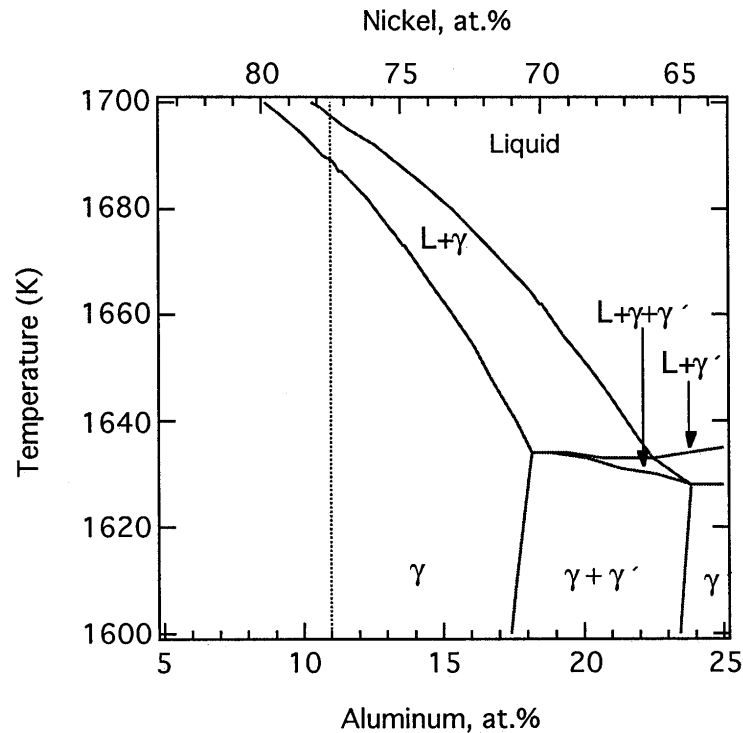
Nickel, at.%

Fig. 10. A quasi–binary diagram of the Ni–Al–Cr system with 11.5 at. %Cr calculated by the Thermo Calc™ program [46].

3.2 Microstructure Development in Nickel-Base Super Alloy Welds

It has long been recognized that the weldability of Ni-base single-crystal superalloy will play a vital role in determining the feasibility of repair welding of land-based gas turbine components. As a result, modeling and characterization of microstructure development in Ni-base superalloy welds has gained importance[55]. Babu et al[55] studied the microstructure development in an electron-beam-welded PWA-1480 single-crystal. A transmission electron micrograph (see Fig. 9) shows a boundary between two dendrite arms. Along the interdendritic regions, large γ', precipitates interlaced by thin films of γ phase were observed. The morphology of these large γ', precipitates with penetrated γ phase suggests that these γ' precipitates formed during the final stages of solidification through the eutectic reaction, L → γ + γ', In many occasions, Laves phases were also observed along the inter-dendritic regions. Within the core of the dendrite, much finer, cuboidal L1$_2$-ordered

γ', precipitates were observed. The above micro-structural development can be explained with the help of a quasi-binary diagram of the Ni- Al-Cr alloy system, as shown in Fig. 10.

To illustrate the microstructural development in the PWA- 1480 alloy, the phase changes in the Ni-11.0 at. % Al-11.5 at. % Cr alloy, as it solidifies from the liquid state, are discussed below. According to the equilibrium phase diagram, the solidification to γ starts at ~ 1698K and is completed at ~ 1685 K. Since the weld cooling conditions are far from equilibrium conditions, this may not be an actual representation of the weld solidification. The variations in the compositions of the γ matrix and liquid phase during such a solidification in an Ni-11.0 at. % Al-11.5 at. % Cr alloy, (assuming Scheil's model) were calculated using the ThermoCalc™ software[55]. The calculations indicate that the solidus temperature (liquid fraction ~ 0.01) is lowered by 50 K, i.e., to 1635 K. ThermoCalc™ calculations also indicate that the final liquid, due to solute enrichment, will undergo a eutectic reaction below
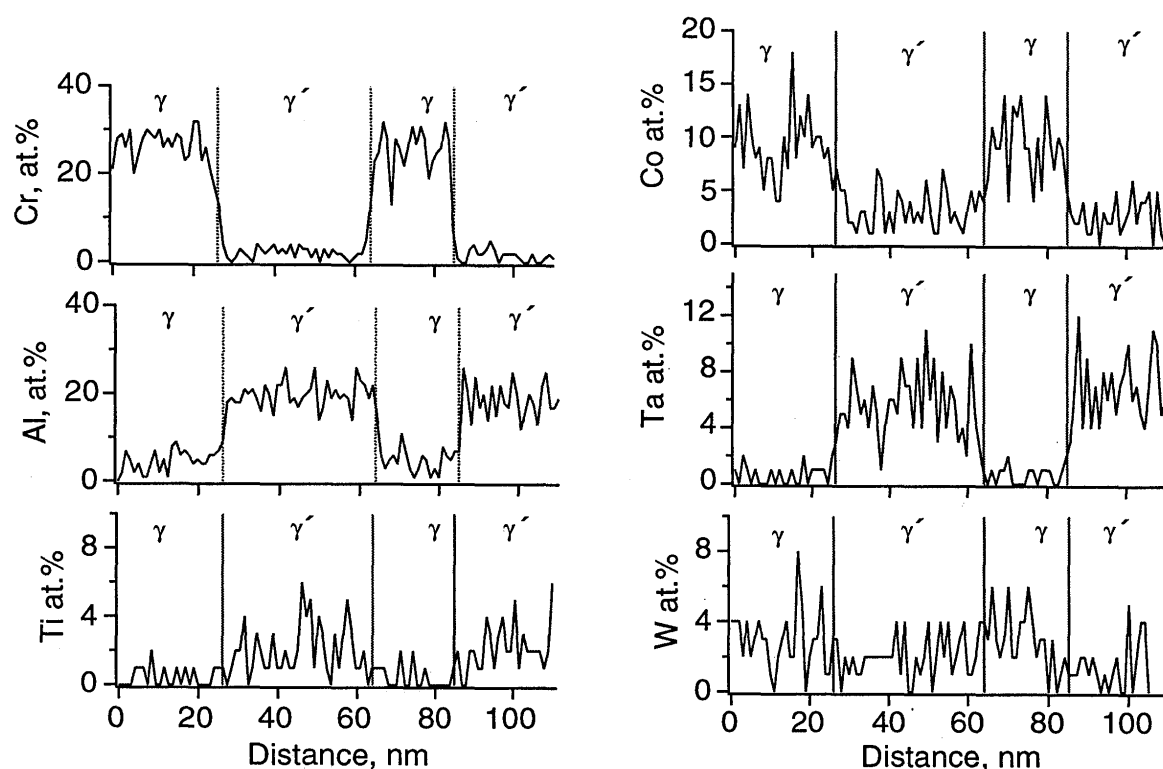
Fig. 11. Atom probe concentration profiles (in at. %) of Cr, Al, Ti, Co, Ta, and W obtained from the PWA – 1480 weld sample. These plots show the variation of elemental concentration through γ(Cr–rich) and γ′ (Al–rich) phases. It is noteworthy that the resolution of this analysis is on a nanometer scale.

1630 K as shown in Fig. 10. The observation (see Fig. 9) of large γ′, precipitates interlaced with films of the γ phase supports this mode of solidification for the weld. However, this work[55] is only approximate, since Ti, Ta, W, and Co will modify the partitioning characteristics between the γ and γ′, phases. Therefore, one has to use other calculation methods[56] or apply the most recent thermodynamic data for the calculations.

In addition to modeling the phase changes during solidification, it is important to consider the solid state decomposition in these welds. On cooling below the solidus temperature, the γ′, phase is expected to precipitate homogeneously within the γ dendrites. It is speculated that, due to the rapid cooling conditions in electron beam welding, the partitioning between γ and γ′, phases may lead to some interfacial segregation of elements such as tungsten and tantalum[55]. To validate the above speculation and to aid in the modeling of microstructural evolution, atom-probe field-

ion microscopy (APFIM) was used to characterize the compositional distribution on an atomic scale. The details of this study can be seen in reference 55. The APFIM results indicated that the compositions of γ and γ′, phases from welds are more or less similar to those of base metal γ and γ′, phases. The high-resolution chemical analysis in APFIM (see Fig. 11) failed to show any interfacial segregation. It is noteworthy that the alloying elements, despite the rapid weld cooling conditions, partition between the γ and γ′, phases. The heavy elements such as tantalum and tungsten, which are expected to diffuse slowly, are also found to partition during weld cooling. These results suggest that the kinetics of the decomposition of γ phase to a mixture of γ and γ′ phases are rapid. Further work is under way to study the partitioning in laser welding, which may induce a higher cooling rate than the electron beam welding process. This information will be utilized in the development of thermo-dynamic and kinetic models to describe the phase transformations in Ni-base superalloy welds.

4. SUMMARY

This paper discusses theoretical, nume-rical, and physical modeling activities to describe physical processes that occur in the weld metal region. This overview indicates that it is indeed possible to develop a generalized model for prediction of weld metal microstructure development, as a function of weld metal composition and welding process parameters, for any alloy system. This paper illustrates the sequential dependency of each of the physical processes in a typical welding situation with microstructural evolution in low-alloy steel and Ni-base superalloy single-crystal welds. The importance of the fundamental understanding of the mechanisms of physical processes in welds and the validation of models with advanced experimental tools, such as APFIM are also emphasized.

ACKNOWLEDGMENTS

REFERENCES

1) T. DebRoy and S. A. David: Rev. Mod. Phys., 67 (1995), p. 85.

2) J. Szekely: Advances in Welding Science and Technology, ed. S. A. David, ASM, Materials Park, Ohio, (1986), p. 3.

3) T. DebRoy: Mathematical Modeling of Weld Phenomena, ed. H. Cerjak and K. E. Easterling, The Institute of Materials, London, (1993), P. 24.

4) S. A. David and J. M. Vitek: Mathematical Modeling of Weld Phenomena, ed. H. Cerjak and K. E. Easterling, The Institute of Materials, London, (1993), p. 41.

5) S. A. David and J. M. Vitek: Int. Mater. Rev., 34 (1989), p. 213.

6) D. L. Olson, S. Liu, and G. R. Edwards: Mathematical Modeling of Weld Phenomena, ed. H. Cerjak and K. E. Easterling, The Institute of Materials, London, (1993), p. 89.

7) H. K. D. H. Bhadeshia and L.-E. Svensson: Mathematical Modeling of Weld Phenomena, ed. H. Cerjak and K. E. Easterling, The Institute of Materials, London, (1993), p. 109.

8) K. E. Easterling: Mathematical Modeling of Weld Phenomena, ed. H. Cerjak and K. E. Easterling, The Institute of Materials, London, (1993).p. 183.

9) S. A. David, J. M. Vitek, T. Zacharia, and T. DebRoy: Proc. of Physical Aspects of ArcWelding, International Institute of Welding, Glasgow, United Kingdom, Sep. 1, (1993), p. 95.

10) S. A. David, J. M. Vitek, S. S. Babu, and T. DebRoy: Proc. of 42nd National Welding Conference, Vol. 2., Welding Technology Institute of Australia, Silverwater, New SouthWales, Australia, (1994).

11) J. C. Villafuerte, H. W. Kerr, and S. A. David: Mater. Sci. Eng., A194 (1995), p. 187.

12) K. Mundra, T. DebRoy, S. S. Babu, and S. A. David: Trends in Welding Research, Gatlinburg, Tennessee, June 5-8, (1995).

13) T. Zacharia and S. A. David: Mathematical.Modeling of Weld Phenomena, ed. H. Cerjak and K. E. Easterling, The Institute of Materials, London, (1993), p. 3.

14) M. Rappaz and Ch.-A. Gandin, Acta Metall. Mater., 41 (1993), p. 345.

15) Ch.-A. Gandin, M. Rappaz, and R. Tintillier: Metall. Trans. A., 24A (1993), p. 467.

16) W. B. Dress, T. Zacharia, and B. Radhakrishnan: Modeling and Control of Joining Processes, ed. T. Zacharia, American Welding Society, Miami, Fla., 1994) p. 321.

17) W. Kurz and D. J. Fisher: Fundamentals of Solidification, Trans Tech., Aedermannsdorf, Switzerland, (1989).

18) M. C. Flemings: Solidification Processing, McGraw-Hill, New York, (1974).

19) S. S. Babu, H. K. D. H. Bhadeshia, and L.-E. Svensson: J. Mater. Sci. Lett., 10 (1991), p. 142.

20) J. A. Brooks and M. I. Baskes: Advances in Welding Science and Technology, ed. S. A. David, ASM, Materials Park, Ohio, (1986) p. 93.

21) T. Matsumiya, T. Koseki, W. Yamada, and Y. Ueshima: Nippon Steel Technical Report, 57 (1993), p. 50.

22) E. Scheil: Z. Metall., 34 (1942), p. 70.

23) M. Rappaz, S. A. David, J. M. Vitek, and L. A. Boatner: Metall. Trans, A., 20A (1989), p. 1125.

24) M. Rappaz, S. A. David, J. M. Vitek, and L. A. Boatner: Metall. Trans. A., 21A (1990), p. 1767.

25) S. A. David, J. M. Vitek, M. Rappaz, and L. A. Boatner: Metall. Trans, A., 21A (1990), p. 1753.

26) M. Rappaz, S. A. David, J. M. Vitek, and L. A. Boatner: Metall. Trans, A.,, 24A (1993) p. 1433.

27) S. A. David and J. M. Vitek: Lasers in Metallurgy, ed. K. Mukerjee and J. Mazumder, TMS, Warrendale, Pa., (1981), p. 2247.

28) J. M. Vitek, A. DasGupta, and S. A. David: Metall. Trans.A, 14A (1983), p. 1833.

29) S. A. David, J. M. Vitek, and T. L. Hebble: Weld. J., 66 (1987), p. 289s.

30) S. Katayama and A. Matsunawa: Proc. ICALEO, (1984), p. 60.

31) J. W. Elmer, S. M. Allen, and T. W. Eagar: Metall. Trans. A., 20A (1989), p. 2117.

32) W. Kurz: Trends in Welding Research, Gatlinburg, Tennessee, June 5-8, (1995).

33) H. K. D. H. Bhadeshia, L.-E. Svensson, and B. Gretoft: Acta Metall., 33 (1985) p.1271.

34) Y. Chen, B. Radhakrishnan, and R. G. Thompson: International Trends in Welding Science and Technology, ed. S. A. David and J. M. Vitek, ASM, Materials Park, Ohio, (1993), p. 259.

35) B. Radhakrishnan and T. Zacharia: Modeling and Control of Joining Processes, ed. T. Zacharia., American Welding Society, Miami, Fla., (1994), p. 298.

36) J. C. Ion, K. E. Easterling, and M. F. Ashby: Acta Metall., 32 (1984), p. 1949.

37) J. M. Race and H. K. D. H. Bhadeshia: International Trends in Welding Science and Technology, ed. S. A. David and J. M. Vitek, ASM, Materials Park, Ohio, (1993), p. 315.

38) J. M. Vitek, S. A. David, D. J. Alexander, J. R. Keiser, and R. K. Nanstad: Acta Metall. Mater., 39 (1991), p. 503.

39) J. W. Christian: The Theory of Transformations in Metals and Alloys - Part I Equi-librium and General Kinetic Theory, 2nd ed., Pergamon Press, New York, (1981).

40) J. M. Vitek, S. A. Vitek, and S. A. David: Metall. Mater. Transa. A., 26A (1995), p.2007.

41) B. Radhakrishnan and T. Zacharia: Metal. Mater. Trans. A., 26A (1995), p. 167.

42) B. Radhakrishnan and T. Zacharia: Metall. Mater. Trans. A., 26A (1995), p. 2123.

43) Ø. Grong: Fourth International Conference on Trends in Welding Research, Gatlinburg, Tennessee, June 5-8, (1995).

44) H. K. D. H. Bhadeshia: Bainite In Steels, Institute of Materials, London, (1992).

45) S. Suzuki, G. I. Rees and H. K. D. H. Bhadeshia: Modeling and Control of Joining Processes, T. Zacharia Ed., American Welding Society, Miami, Fla., (1994), p. 186.

46) S. S. Babu and H. K. D. H. Bhadeshia: Mater. Sci. and Eng., A156 (1992), p.1

47) B. Sundman, B. J. Jansson, and J.O. Anderson : Calphad, 9 (1985), p. 153.

48) S. A. David, T. DebRoy, and J. M. Vitek: MRS Bull., XIX (1994), p. 29.

49) S. A. David and T. DebRoy: Science, 257 (1994), p. 497.

50) A. Kluken and Ø. Grong: Metall. Trans. A., 20A (1989), p. 1335.

51) F-C. Liao and S. Liu: Weld. J., 71 (1992), p. 94s.

52) S. S. Babu, S. A. David, J. M. Vitek, K. Mundra, and T. DebRoy: Mater. Sci.Technol., 11 (1995), p. 186.

53) K. Mundra, T. DebRoy, S. S. Babu, and S. A. David: submitted for publication in Weld. J., (1995).

54) S. S. Babu, S. A. David, J. M. Vitek, K. Mundra and T. DebRoy: Trends in Welding Research, Gatlinburg, Tennessee, June 5-8, (1995).

55) S. S. Babu, S. A. David, and M. K. Miller: APPI. Surf. Sci., 94/95 (1996), p. 280.

56) M. Enomoto, H. Harada, and M. Yamazaki: Calphad, 15 (1991), p. 143.